

# Dynamic power flow based simplified transfer function model to study instability of low-frequency modes in inverter-based microgrids

ISSN 1751-8687

Received on 29th April 2020

Revised 23rd July 2020

Accepted on 3rd September 2020

E-First on 19th October 2020

doi: 10.1049/iet-gtd.2020.0818

www.ietdl.org

Ayesha Firdaus<sup>1</sup> ✉, Dushyant Sharma<sup>2</sup>, Sukumar Mishra<sup>1</sup><sup>1</sup>Department of Electrical Engineering, Indian Institute of Technology Delhi, Hauz Khas, New Delhi, India<sup>2</sup>Department of Electrical Engineering, Indian Institute of Technology Jodhpur, Rajasthan, India

✉ E-mail: ayeshafirdaus11@gmail.com

**Abstract:** This study proposes a new modelling approach for studying low-frequency oscillations (LFOs) in a droop controlled islanded microgrid. Due to the absence of inertia, these sources are more vulnerable to power and frequency oscillations. Their quick response can introduce faster electrical dynamics in the system which should be monitored from time to time. To ease the analysis process, this study proposes a simplified method for finding LFO in the microgrid. Inspired from the small-signal automatic generation control model of the conventional grid, a transfer function based closed-loop small-signal model of inverter-based islanded microgrid is presented in this study to study power-sharing among the various inverters. The proposed model uses the concept of dynamic power flow through the network to find the power output of each source following load perturbations in a system. Time domain simulation results and eigenvalue analysis is provided to verify the effectiveness of the proposed small-signal model. By comparing the results obtained with actual system simulation in MATLAB/Simulink, it is found that the proposed simplified model is able to predict the stability margin and the LFO of the system without using actual detailed state-space modelling procedure.

## Nomenclature

$v_{id}, v_{iq}$	$dq$ components of inverter voltage
$v_{id}^*, v_{iq}^*$	$dq$ components of reference voltage of inverter
$v_{Td}^*, v_{Tq}^*$	$dq$ components of reference output voltage of inverter
$v_{Td}, v_{Tq}$	$dq$ components of output voltage of inverter
$i_{Ld}^*, i_{Lq}^*$	reference $dq$ components of coupling inductor current
$i_{Ld}, i_{Lq}$	$dq$ components of coupling inductor current
$i_{Td}, i_{Tq}$	$dq$ components of output current of inverter
$i_{LineDQ}$	$dq$ components of connecting line currents
$i_{LoadDQ}$	$dq$ components of load currents
$v_{bDQ}$	$dq$ components of bus voltage
$m_p, n_q$	active and reactive power droop coefficients
$\omega_n$	nominal frequency set point of DG
$V_n$	nominal $d$ -axis voltage set point of DG
$F$	feed-forward gain of voltage controller
$\omega$	operating frequency of DG
$\omega_{ref}$	frequency of reference frame
$\delta$	difference of angle between the individual reference frame and common reference frame
$P_{ins}, Q_{ins}$	instantaneous value of active and reactive power
$P_{fun}, Q_{fun}$	average value of active and reactive power
$x_{MG}$	microgrid states
$P_{inii}, Q_{inii}$	initial value of active and reactive power supplied by $i$ th inverter
$P_{cali}, Q_{cali}$	$i$ th inverter instantaneous active and reactive power after lag of digital control
$A_{MG}$	microgrid state matrix
$\tilde{p}_{i,j}, \tilde{q}_{i,j}$	active and reactive power through a line connecting bus $i$ and $j$
$S_{pv}, S_{pd}$	dynamic phasor coefficients for calculation of active power
$S_{qv}, S_{qd}$	dynamic phasor coefficients for calculation of reactive power
$\Delta P_{Li}$	resultant initial load power shared by the $i$ th inverter
$P_{Li}^j$	initial contribution of $i$ th inverter to $j$ th load

## 1 Introduction

In microgrids, distributed generations (DGs) are extensively used to supply power from renewable energy sources. These DGs supply power to the locally distributed loads through voltage source inverters. These power electronic-based technologies improve the control capabilities of DGs. However, due to the absence of inertia as compared to conventional generators, these microgrids have reduced stability margins [1]. Therefore, following a fault or a disturbance, either small or large, these systems give rise to different modes of oscillations. For the islanded operation of microgrids, droop control method is extensively used for power-sharing among sources as it does not require a communication link to control. Inverter-based DGs operate in parallel under droop algorithm to supply load while maintaining bus voltages and system frequency [2].

State-space small-signal analysis is well established in the literature for the study of oscillations in conventional systems. It has also been used extensively for the past decade in microgrids to obtain various frequency modes [3]. In [4, 5], a detailed state-space model for stability analysis of inverter-based islanded microgrid with passive loads is presented and the same has been widely followed. After this model, many studies have been presented in the literature to model droop controlled islanded microgrids. In [6, 7], the impact of induction motor and converter type loads on microgrid stability are presented, respectively. Different heterogeneous droop schemes are compared in [8] based on their transient performance. These studies conclude that various frequency modes in islanded microgrids are divided into three separate time scales. Higher and medium frequency modes are mainly affected by the filter and the voltage and current controller parameters. On the other hand, low-frequency modes are affected by the droop controller, network configuration, cut-off frequency of power filters and loading conditions [9]. The former modes of two groups are much damped as compared to later low frequency group which affects stability margins of a microgrid. The lightly damped low-frequency oscillations (LFOs) can lead to large power oscillations in the system making it unstable [10]. Many controllers have been proposed to damp these oscillations for improving the

stability margins of a microgrid [11–14]. Studies based on optimisation of droop controller parameters for improved transient response are also presented in [15–17]. The literature mentioned so far make use of state-space small-signal representation based stability analysis which accurately computes the system oscillations. However, such type of analysis is very complex especially for inverter-based DG systems. This is because of the fact that such systems involve detailed modelling due to the electrical time constants associated with them. It involves a large number of differential equations and algebraic equations to be linearised and solved for calculating different frequency modes which increases the dimensionality of the model and makes the process computationally difficult for larger systems. Hence the process of deciding the stability margin for the inverter-based systems and obtaining the frequency modes becomes quite complex.

To solve the aforementioned problem related to a detailed modelling approach, many authors have come up with model order reduction (MOR) techniques for simpler analysis such that only those states which affect the LFO are considered in modelling and rest others are neglected. In [18–20], authors have presented a reduced-order model for inverter-based microgrids using singular perturbation theory. Krons reduction of network-based reduced-order model is presented in [21, 22] for stability analysis of such systems. The various MOR techniques have reduced the order of system state matrix, however, reducing states still require further computations like calculation and inversion of state matrix. Moreover, these techniques give results with lesser accuracy [23].

In microgrids which are converter dominated, network dynamics also play a vital role in the low-frequency dynamics as the power output of each inverter is actually dependent on the network dynamics and hence, it is essential to include network dynamics in such studies [23]. In [23], keeping in view the importance of network dynamics, a concept of the dynamic phasor is applied to predict the stability margin of two droop controlled inverters. The dynamic phasor approach proposed in [23] is much simpler than MOR techniques and also, it is fair enough in predicting the stability margin. However, the model is not generalised enough to be applied on any larger systems having multiple inverters and loads at different connection points in a microgrid. The model proposed in [23], computes the stability of the system when two inverters are connected to a common bus. The dynamics of the inverters are presented with reference to the common bus but the model is not extended to study the dynamics of the inverters with each other for a system having multiple inverters connected at different buses. In view of the above, the following points can be concluded as the limitations of the existing modelling methods.

- The development of the small-signal model of a complete microgrid is a complex mathematical process and the complexity increases with increase in the number of inverters, lines, and loads. Due to the fast nature of static sources, the network needs to be considered as well in the small-signal study. This leads to the requirement of linearisation of a large number of state equations and the system becomes complex.
- MOR techniques can help in reducing the number of states but the mathematical complexity is still there. Further, these techniques give results with lesser accuracy [23].
- Although [23] presents a simple yet accurate method to include the dynamics of the network in a simplified model, the dynamic phasor based method presented in [23] studies only the interaction of the sources with a reference bus. However, the power oscillations in a droop controlled microgrid are seen among the sources where one source oscillates with respect to others. This is not studied in [23]. It is shown further in this paper that observing the dynamics with reference to a fixed bus may give inaccurate results if the bus magnitude and angle are not maintained constant. The authors' believe that the philosophy may work in grid-connected systems as the grid maintains the bus voltage magnitude and angle, but the same may not give accurate results in autonomous systems.

- Further, in [23] the sources are assumed to be connected to a common bus whose voltage is assumed as the reference. As discussed previously, the same may give erroneous results. Moreover, in a practical system, all sources may not be connected to a common bus and therefore, LFO for any general microgrid may not be studied by this method alone.

- In [23], the power sharing at the instant of load perturbation is not discussed. In what proportion the load power is supplied by each source at the instant of load perturbation impacts the system dynamics. The same is missing in [23]. To the best of authors' understanding, there is not enough literature that presents how power is shared among multiple sources at the instant of load perturbation followed by the dynamics that make the power equal or that make the system stable/unstable as per the droop coefficient.

- Reference [23] also does not consider a transfer function to account for the delay in the measurement of quantities and achieving the desired control. It is shown further in this paper that this transfer function plays a critical role in modelling the system dynamics with the dynamic phasor model.

### 1.1 Contribution

Keeping the above-mentioned challenges in view, the contribution of the present work is to develop a new model to study the LFO in an inverter-based microgrid which addresses the following objectives:

- To develop a model which is simple in implementation, and mathematical complexity needed to develop the same is reduced.
- To develop a model which enables the study of both initial power outputs of the sources and the steady-state results and also, enables both time-domain and frequency-domain studies as the proposed model is a linearised model.
- To develop a model which can study the interaction among all the sources in the microgrid and at the same time, which is generalised and which can be easily be extended if the number of sources change.

Bridging the gaps of model developed in [23] and to meet the objectives mentioned above, authors have proposed a transfer function based closed loop simplified model to study the LFO. Concept of dynamic phasors can be extended to obtain the dynamic power flows through various lines in the network with load perturbations at different connection points. Thus, interaction among various inverters through connecting lines can be obtained based on these dynamic power flows. The proposed model is not based upon any MOR techniques, rather this method directly develops a simplified model which only takes into consideration the system dynamics which are responsible for LFO and thus making it simpler as compared to other methods developed in literature so far. The proposed model is inspired by the well-known automatic generation control (AGC)/automatic load frequency control model in which change in tie-line power flow is obtained based on the difference in angles of the buses as a result of the frequency difference in the two areas to which the tie-line is connected. The change in tie-line power flow adds to the source in one area while it adds to the load in the other area [24, 25]. This concept is used to calculate the power flow between two inverter-based sources and then the change in power flow adds as a load to one inverter while it adds as a source (negative load) to the other inverter.

### 1.2 Organisation

The rest of the paper is organised as follows. Section 2 contains test microgrid description and its control architecture used for simulation. The small signal and sensitivity analysis based on conventional approach is presented in Section 3. Section 4 presents step by step procedure to develop the proposed simplified small signal model for stability analysis. Time domain and frequency domain results are presented in Section 5 followed by conclusion of the paper in Section 6.

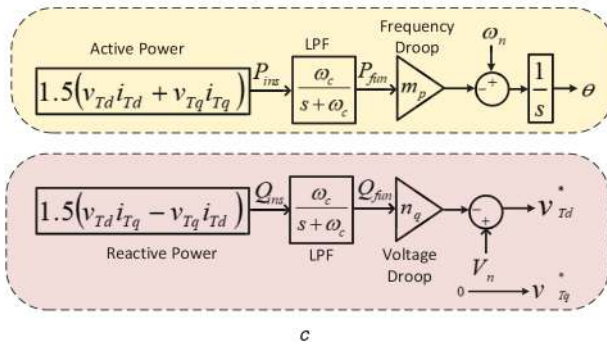
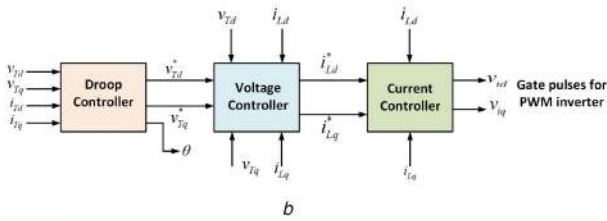
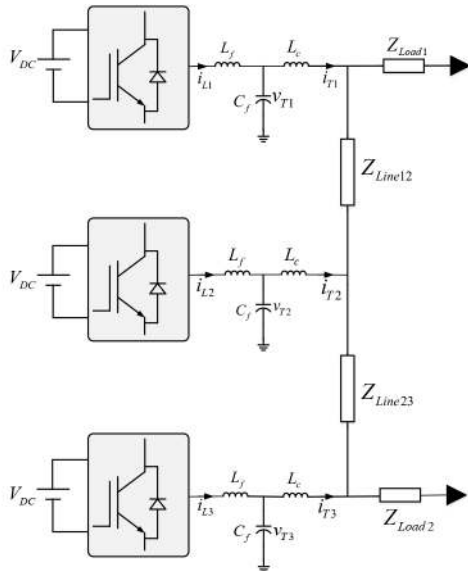


**Fig. 1** Test microgrid with inverter controls  
(a) Test system under study, (b) Block diagram of inverter control, (c) Droop controller

## 2 Test system structure and mathematical modelling

The simulated microgrid is a 220 V per phase RMS, 50 Hz three phase system as shown in Fig. 1a. The test system parameters are given in Table 1. It consists of three inverter-based DGs which are working in parallel to maintain frequency and bus voltages in the system. The frequency and voltage droop based primary control is used for firing inverters which supply two passive loads connected at bus 1 and 3. The overall control philosophy for autonomous inverters used for simulation is same as given in [10]. The complete block diagram of inverter control is shown in Fig. 1b. To avoid redundancy, only relevant equations and schematic are shown and complete control structure can be found in [10].

The instantaneous power at the output of the inverter is calculated and then passed through a low pass filter to extract the fundamental component. The resultant power is now given to the droop controller for obtaining reference frequency and voltage for an individual inverter as shown in Fig. 1c. The governing equations are given as:

$$\begin{aligned} \omega &= \omega_n - m_p * P_{\text{fun}} \\ v_{Td}^* &= V_n - n_q * Q_{\text{fun}} \end{aligned} \quad (1)$$

**Table 1** Test system parameters

Parameter	Notation	Value
resistance of output filter	$R_f$	0.1 $\Omega$
inductance of output filter	$L_f$	1.35 mH
capacitance of output filter	$C_f$	50 $\mu\text{F}$
resistance of coupling branch	$R_c$	0.03 $\Omega$
inductance of coupling branch	$L_c$	0.35 mH
impedance of line 1	$Z_{\text{Line12}}$	0.23 + 0.1j $\Omega$
impedance of line 2	$Z_{\text{Line23}}$	0.35 + 0.58j $\Omega$
voltage controller proportional gain	$K_{pv}$	0.1682
voltage controller integral gain	$K_{iv}$	189.345
current controller proportional gain	$K_{pc}$	13.5716
current controller integral gain	$K_{ic}$	1005.310
cut-off frequency of low pass filter	$\omega_c$	31.41 rad/s

where  $\omega$  and  $v_{Td}^*$  are the new reference frequency and voltage, respectively, after introducing droop into the nominal quantities  $\omega_n$  and  $V_n$ . The voltage reference for  $q$ -axis is assumed to be zero so that output voltage magnitude would be aligned with  $d$ -axis of the inverter reference frame [4, 5]. Active and reactive power droop coefficients are represented by  $m_p$  and  $n_q$ , respectively, which are defined as the change in frequency and voltages per unit rated power of the DG.  $P_{\text{fun}}$  and  $Q_{\text{fun}}$  are fundamental power obtained from a low pass filter as given by:

$$P_{\text{fun}} = \frac{\omega_c}{s + \omega_c} * (P_{\text{ins}}) \quad (2)$$

$$Q_{\text{fun}} = \frac{\omega_c}{s + \omega_c} * (Q_{\text{ins}})$$

The instantaneous power used in the above relation ( $P_{\text{ins}}$  and  $Q_{\text{ins}}$ ) can be calculated using the sensed value of voltage and current at the output of the inverter terminal as shown in Fig. 1c. The references generated by the droop controller is given to voltage controller for maintaining bus voltages followed by current control loop which limits the input current to the switches. The voltage and current controllers are standard proportional-integral (PI) regulators. Equations related to these control loops are defined as:

$$\dot{i}_{Ld}^* = F i_{Ld} - \omega C_f v_{Tq} + G_v(s)(v_{Td}^* - v_{Td}) \quad (3)$$

$$\dot{i}_{Lq}^* = F i_{Lq} + \omega C_f v_{Td} + G_v(s)(v_{Tq}^* - v_{Tq}) \quad (4)$$

$$v_{Td}^* = -\omega L_f i_{Lq} + G_f(s)(i_{Ld}^* - i_{Ld}) \quad (5)$$

$$v_{Tq}^* = \omega L_f i_{Ld} + G_f(s)(i_{Lq}^* - i_{Lq}) \quad (6)$$

where  $v_T$  is the capacitor terminal voltage of inverter,  $i_L$  is the inverter output current,  $F$  is the feed forward term, and  $G_v(s)$  and  $G_f(s)$  are the transfer function of standard PI regulator given as:

$$G_v(s) = K_{pv} + K_{iv}/s; \quad G_f(s) = K_{pc} + K_{ic}/s \quad (7)$$

Neglecting switching dynamics, inverter output voltage ( $v_{idq}$ ) is assumed to be equal to its reference value ( $v_{idq}^*$ ). The current and voltage dynamics of LCL filter in local reference frame at the inverter terminals are defined as:

$$v_{id} - v_{Td} = (R_f + sL_f)i_{Ld} - \omega L_f i_{Lq} \quad (8)$$

$$v_{iq} - v_{Tq} = (R_f + sL_f)i_{Lq} + \omega L_f i_{Ld} \quad (9)$$

$$\dot{i}_{Ld} - i_{Td} = sC_f v_{Td} - \omega C_f v_{Tq} \quad (10)$$

$$\dot{i}_{Lq} - i_{Tq} = sC_f v_{Tq} + \omega C_f v_{Td} \quad (11)$$

$$s i_{Tdqi} = (-R_c/L_c) i_{Tdqi} \pm \omega i_{Tdqi} + (1/L_c)(v_{Tdqi} - v_{bdqi}) \quad (12)$$

Connecting lines and passive loads are modelled as series RL branches. The dynamical equations for the same are described on a network reference frame as given in (13) in (14), respectively

$$s i_{LineDQi} = (-R_{Line}/L_{Line}) i_{LineDQi} \pm \omega i_{LineDQi} + (1/L_{Line})(v_{bDQj} - v_{bDQk}) \quad (13)$$

$$s i_{LoadDQi} = (-R_{Load}/L_{Load}) i_{LoadDQi} \pm \omega i_{LoadDQi} + (1/L_{Load}) v_{bDQi} \quad (14)$$

The complete microgrid is described by the mathematical model given from (1) to (14) and this model will be used for detailed small signal analysis discussed subsequently.

### 3 Detailed small signal state space analysis approach

The conventional state space analysis is based on the Taylor series expansion of non-linear differential equations to form a linearised set of equations. For a linear time-invariant system with  $p$  inputs,  $q$  outputs and  $n$  state variables, the state-space representation is given in (15):

$$\begin{aligned} \dot{\mathbf{x}}(t) &= \mathbf{A}\mathbf{x}(t) + \mathbf{B}\mathbf{u}(t) \\ \mathbf{y}(t) &= \mathbf{C}\mathbf{x}(t) + \mathbf{D}\mathbf{u}(t) \end{aligned} \quad (15)$$

where  $\mathbf{x}(t)$  is the state vector,  $\mathbf{y}(t)$  is the output vector,  $\mathbf{u}(t)$  is the input/control vector,  $\mathbf{A}$  is the state/system matrix of the order  $n \times n$ ,  $\mathbf{B}$  is the input matrix of the order  $n \times p$ ,  $\mathbf{C}$  is the output matrix of the order  $q \times n$  and  $\mathbf{D}$  is the feedforward matrix of the order  $q \times p$

For developing the system state matrix, first, state space model of multiple inverters, lines and loads are obtained. Then state space model of individual components are combined on a common reference frame. Any frame can be selected as a common reference frame and all other frames are converted to the reference frame by using (17) where, the angle  $\delta$  which is required for transformation can be obtained using (16).  $\delta_i$  describes the angle between common reference frame and individual reference frame for the  $i$ th inverter.

$$\delta = \int (\omega - \omega_{ref}) dt \quad (16)$$

$$f_{DQ} = T_i f_{dq} \quad (17)$$

where  $f_{dq}$  represents the states in individual reference frame,  $f_{DQ}$  is the representation of the same on the common reference frame and  $T_i$  is the transformation matrix given by (18)

$$T_i = \begin{bmatrix} \cos(\delta_i) & -\sin(\delta_i) \\ \sin(\delta_i) & \cos(\delta_i) \end{bmatrix} \quad (18)$$

In this paper, the inverter 1 frequency is selected as the common frame. To obtain the state-space model of the complete microgrid, (1)–(14) are linearised around an operating point and combined on a common frame to get the complete state matrix as given in (19).

$$\Delta \dot{\mathbf{x}}_{MG} = A_{MG} * \Delta \mathbf{x}_{MG} \quad (19)$$

The state variables given in (19) are

$$\Delta \mathbf{x}_{MG} = [\Delta \mathbf{x}_{inv}, \Delta \mathbf{x}_{Line}, \Delta \mathbf{x}_{Load}]^T$$

where

$$\begin{aligned} \Delta \mathbf{x}_{inv} &= \{ \Delta P_{fun}, \Delta Q_{fun}, \Delta \delta, \Delta \phi_{dq}, \Delta \psi_{dq}, \\ &\quad \Delta v_{Tdq}, \Delta i_{Ldq}, \Delta i_{Tdqi} \} \\ \Delta \mathbf{x}_{Line} &= \{ \Delta I_{Linedq} \} \\ \Delta \mathbf{x}_{Load} &= \{ \Delta I_{Loaddq} \} \end{aligned}$$

Each inverter will have states corresponding to power control ( $\Delta P_{fun}$ ,  $\Delta Q_{fun}$ ,  $\Delta \delta$ ), voltage control ( $\Delta \phi_{dq}$ ), current control ( $\Delta \psi_{dq}$ ) and filter parameters ( $\Delta v_{Tdq}$ ,  $\Delta i_{Ldq}$ ). As discussed previously, the network ( $\Delta I_{Linedq}$ ) and load ( $\Delta I_{Loaddq}$ ) dynamics also play a part in the overall system studies. Therefore, as the number of sources/lines/loads increase in the system, the number of states also increase. For each new droop controlled inverter, there are 13 new states. Thus, it becomes a very computational analysis as the number of inverter increases.

The overall system state matrix ( $A_{MG}$ ) is a  $47 \times 47$  matrix which is represented in the form of various symbols and sub-matrices. The complete matrix is not presented in this paper due to space constraints and it can be seen in [4].

#### 3.1 Eigen value analysis

By using system state matrix ( $A_{MG}$ ), eigen values of the system are obtained and their spectrum is shown in Fig. 2. There are three sets of modes: high-frequency, medium-frequency and low-frequency modes. Out of the three, damping of high and medium frequency modes is sufficient to keep the system stable. However, damping of some low-frequency modes is not sufficient and hence they are responsible for making system unstable at different operating conditions. These critical low-frequency modes are shown in Table 2. It can be seen in Table 2 that the critical oscillatory mode is close to 8 Hz. The frequency of oscillation in droop controlled microgrid is higher as compared to typical LFO range in large power grid due to the faster electrical dynamics and lesser inertia of inverter. The LFO in a large power grid could be of various types ranging from 0.1–2.5 Hz, e.g. local plant mode, intermachine or interplant mode, interarea mode, control mode etc. [24]. The LFOs, on the other hand, in a droop controlled microgrid are due to the lag introduced by the low pass filter delay which causes a delayed change in frequency of the inverter when its power changes due to change in load [10]. This leads to the supply of power from a source which is generating the voltage at a higher frequency to other nearby sources at a relatively lower frequency. Thus, the oscillations are seen among the power and frequency of one source against the other nearby source and effectively all the sources swing against each other like the interplant mode in large power systems. In a droop controlled microgrid these oscillations can range around 5–15 Hz [4–13].

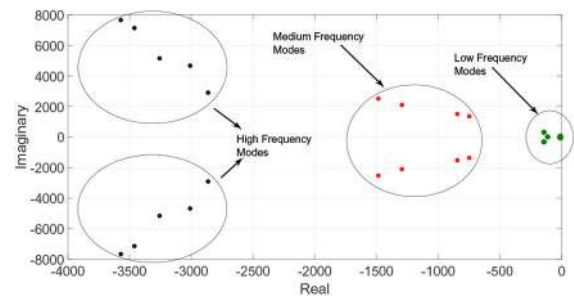


Fig. 2 Eigen value spectrum of microgrid under study

Table 2 Critical low-frequency modes at  $m_p = 1.15 * 10^{-4}$

Mode	Eigen value	Damping ratio, %
mode I	$-0.02 \pm 49.27j$	0.04
mode II	$-12.91 \pm 29.18j$	40

**Table 3** Participation factors of critical low-frequency modes

Mode 1		Mode 2	
States	Participation	States	Participation
$P_1$	0.21	$P_1$	0.14
$Q_1$	0.04	$Q_1$	0.02
$P_2$	0.29	$P_3$	0.38
$Q_2$	0.04	$Q_3$	0.03
$\delta_2$	0.56	$\delta_3$	0.66

### 3.2 Sensitivity analysis

To find the origin of different frequency components, sensitivity analysis is done on system state matrix to observe the participation of different states in a particular mode [24]. The sensitivity factor or participation factor ( $p_{ni}$ ) given in (20) is the measure of relative participation of state variable in a particular mode which is calculated using left and right eigen vectors and is equal to sensitivity of eigen value ( $\lambda_i$ ) to the diagonal element ( $a_{nn}$ ) of the state matrix.

$$p_{ni} = \frac{\partial \lambda_i}{\partial a_{nn}} \quad (20)$$

There are two dominant low-frequency modes which are significantly affected by the droop controller parameters. The actual participation factors given in Table 3 show that the mode-I and mode-II, which are the critical ones (system stability depends on these modes), are mostly dependent on the states of active power loop and  $\delta$  which defines the interconnection of one inverter to the other.

Hence from the analysis done above, it is found that the low-frequency modes caused due to parallel operation of droop controlled inverters are responsible for determining the stability of such type of microgrid. Other control loops do not participate significantly in shaping the critical modes of the system. Therefore, for stability analysis, dynamics of other loops in the inverter control can be neglected and a more simplified model can be obtained.

## 4 Proposed simplified approach for stability analysis

To reduce computational efforts, a simplified small-signal model is developed keeping the fact in mind that only the states of power control loop of the inverter are responsible for low-frequency modes as discussed in Section 3. The proposed interconnected multi-inverter small signal model uses the concept of dynamic phasors as given in [23] to obtain the dynamic power flow through the lines. Dynamic phasors based model has been developed for inverter-based systems to include the dynamics of network elements as well such that the frequency in  $X = \omega L$  is considered to be dynamic and not constant.

The active and reactive power through a line connecting bus  $i$  and  $j$  is expressed as:

$$\begin{aligned} \tilde{p}_{i,j} &= \frac{3}{R^2 + X^2} (Rv_{Ti}^2 - Rv_{Ti}v_{Tj}\cos\delta_{i,j} + Xv_{Ti}v_{Tj}\sin\delta_{i,j}) \\ \tilde{q}_{i,j} &= \frac{3}{R^2 + X^2} (Xv_{Ti}^2 - Xv_{Ti}v_{Tj}\cos\delta_{i,j} - Rv_{Ti}v_{Tj}\sin\delta_{i,j}) \end{aligned} \quad (21)$$

where  $\delta_{i,j} = \delta_i - \delta_j$  is the difference in voltage angle of bus  $i$  and  $j$ .  $v_{Ti}$  and  $v_{Tj}$  are the magnitude of capacitor terminal voltage of inverter  $i$  and inverter  $j$ , respectively.

A complex time domain waveform  $x(t)$  can be represented inside the interval  $\tau \in (t - T, t]$  by the following Fourier series [23, 26]:

$$x(\tau) = \sum_{k=-\infty}^{\infty} X_k(t) e^{jk\omega_s\tau} \quad (22)$$

where  $\omega_s = 2\pi/T$  and  $X_k(t)$  is the Fourier coefficient (time-varying  $k$ th phasor at time  $t$ ) which can be expressed as:

$$X_k(t) = \frac{1}{T} \int_{t-T}^t x(\tau) e^{-jk\omega_s\tau} d\tau = \langle x \rangle_k(t) \quad (23)$$

where  $\langle x \rangle_k(t)$  is the average  $k$ th phase over the period  $T$ .

The derivative of the  $k$ th dynamic phasor can be written as:

$$\frac{dX_k(t)}{dt} = \left( \frac{dx}{dt} \right)_k(t) - jk\omega_s X_k(t) \quad (24)$$

Based on (24), the current through an inductor can be related to the voltage across it as:

$$v_L = L \left( \frac{di_L}{dt} \right) + j\omega L i_L \quad (25)$$

If the derivative in above equation is denoted by the Laplace variable, the real and imaginary part of the impedance of a line containing resistance and inductance is given by  $Ls + R$  and  $\omega L$ , respectively. Using this concept of dynamic phasors, we now have a linear but dynamic model of power flow through a line in which (21) is transformed to:

$$\begin{aligned} \tilde{p}_{i,j} &= 3 \frac{Ls + R}{(Ls + R)^2 + (\omega L)^2} (v_{Ti}^2 - v_{Ti}v_{Tj}\cos\delta_{i,j}) \\ &\quad + 3 \frac{\omega L}{(Ls + R)^2 + (\omega L)^2} v_{Ti}v_{Tj}\sin\delta_{i,j} \\ \tilde{q}_{i,j} &= -3 \frac{Ls + R}{(Ls + R)^2 + (\omega L)^2} v_{Ti}v_{Tj}\sin\delta_{i,j} \\ &\quad + 3 \frac{\omega L}{(Ls + R)^2 + (\omega L)^2} (v_{Ti}^2 - v_{Ti}v_{Tj}\cos\delta_{i,j}) \end{aligned} \quad (26)$$

The linearised equations can be obtained for small disturbances around an operating point as given in:

$$\begin{aligned} \Delta \tilde{p}_{i,j} &= S_{pv} \Delta v_{Ti,j} + S_{pd} \Delta \delta_{i,j} = f(\Delta v_{Ti,j}, \Delta \delta_{i,j}) \\ \Delta \tilde{q}_{i,j} &= S_{qv} \Delta v_{Ti,j} + S_{qd} \Delta \delta_{i,j} = g(\Delta v_{Ti,j}, \Delta \delta_{i,j}) \end{aligned} \quad (27)$$

Equation (27) can be used to calculate dynamic power flow through a line between the buses  $i$  and  $j$  having change in bus voltage magnitude and angle as  $\Delta v_{Ti,j}$  ( $v_{Ti,j} = v_{Ti} - v_{Tj}$ ) and  $\Delta \delta_{i,j}$ , respectively, where

$$\begin{aligned} S_{pv} &= \frac{3(Ls + R)v_{Ti}^0}{(Ls + R)^2 + (\omega L)^2}, & S_{pd} &= \frac{3\omega L(v_{Ti}^0)^2}{(Ls + R)^2 + (\omega L)^2} \\ S_{qv} &= \frac{3\omega L v_{Ti}^0}{(Ls + R)^2 + (\omega L)^2}, & S_{qd} &= \frac{-3(Ls + R)(v_{Ti}^0)^2}{(Ls + R)^2 + (\omega L)^2} \end{aligned}$$

For calculating the dynamic phasor coefficients ( $S_{pd}$ ,  $S_{qd}$ ,  $S_{pv}$  and  $S_{qv}$ ), the net inductance and resistance between  $i$ th and  $j$ th capacitor voltage are used. Due to the very small reactive power droop coefficient ( $n_q$ ), the bus voltages are approximately same i.e.  $v_{T1} \approx v_{T2} \approx v_{T3}$  for small change in reactive power. Hence,  $v_{Ti}^2$  can also be written as  $v_{Ti}v_{Tj}$  and vice versa.

### 4.1 Procedure to develop proposed small signal model

The proposed approach is a generalised one and it can be applied on any size of radial microgrids having passive loads. For the development of the interconnected small-signal model, inverter 1 is considered as the reference frame. The small-signal power flow-based model is obtained for stability analysis which is simpler as that of the model described in Section 3. The step by step

procedure for developing the simplified model is described as follows:

(1) The first step is to initialise each inverter power equal to the amount of load power supplied by that particular inverter bus. As soon as a load is switched ON, the load will extract its current from the shortest impedance path. Therefore, each load just after switching ON will be supplied by different sources in a proportion depending on the net impedance between the inverter and the load. The source which is electrically far from the load will give very small power as compared to the source which is electrically close to the load. For example, in the system shown in Fig. 1a, load 1 is connected at the terminal of bus no. 1. Therefore, as soon as this load is switched ON, it will extract maximum power from inverter 1, some power from inverter 2, and a minimum power (close to zero) from inverter 3. The initial power of each inverter can be obtained by:

$$\Delta P_{\text{inii}} = \Delta P_{L_i} \quad (28)$$

$$\Delta Q_{\text{inii}} = \Delta Q_{L_i} \quad (29)$$

where  $i$  = index of inverter,  $\Delta P_{\text{inii}}$  is the initial power output of the inverter, and  $\Delta P_{L_i}$  is the resultant initial load power shared by the  $i$ th inverter. Similarly, the initial reactive power supplied by each source ( $\Delta Q_{\text{inii}}$ ) is also initialised.

*Initialisation process:* When a load change occurs, as the voltage at each filter capacitor is same, the power demand by the load is supplied by all the sources but in different ratios depending on the electrical distance between the bus where load is connected and the capacitor node of the bus. If the impedance of the coupling inductance and resistance for  $i$ th inverter is given by  $Z_i$  and the impedance of the line connecting bus  $i$  and bus  $j$  is given by  $Z_{ij}$  then the relationships given in the Table 4 define the initial power of each source depending on its electrical distance from the node where the load is connected. The various equivalent impedances  $Z_{\text{eq}i}$  in Table 4 are given in (30).

$$\begin{aligned} Z_{\text{eq}1} &= Z_{12} + [Z_2 \parallel (Z_{23} + Z_3)] \\ Z_{\text{eq}2} &= Z_{23} + Z_3 \\ Z_{\text{eq}3} &= Z_{12} + Z_1 \\ Z_{\text{eq}4} &= Z_2 \parallel (Z_{23} + Z_3) \\ Z_{\text{eq}5} &= Z_{23} + [Z_2 \parallel (Z_{12} + Z_1)] \\ Z_{\text{eq}6} &= Z_{12} + Z_1 \end{aligned} \quad (30)$$

From Table 4, it can be seen that the initial contribution to the load is negligible for the sources which are electrically far and

most of the power is met by the nearest source. This result can prove useful when there are a large number of sources. It can be assumed that the initial contribution for inverters which are far from the load becomes quite close to zero, e.g.  $P_{L3}^1$ . Therefore, when the microgrid is large, for most of the inverters the initial contribution to a few loads will be very small which can be approximated to zero. Thus, it is not needed to calculate the initial contribution from each source. Only the contribution from the sources which are electrically closer needs to be computed. Therefore, this approach does not add much complexity even if the size of the system increases.

Whenever the loads are turned ON, the initial power of each source is calculated as described above and assigned to each inverter. For example, if all the loads ( $P_{\text{Load}1}$ ,  $P_{\text{Load}2}$  and  $P_{\text{Load}3}$ ) are turned ON simultaneously, then the net initial power of the each source is given by:

$$\Delta P_{\text{inii}} = \Delta P_{L_i} = P_{L_i}^1 + P_{L_i}^2 + P_{L_i}^3 \quad (31)$$

Similar expression is used in the case of reactive power and is not written again just to avoid redundancy.

(2) The next step is to find out the change in bus angle and bus voltage for all the inverter buses as per the active and reactive power droop introduced by the power controller. The input to the controller is the change in the instantaneous active and reactive power of the inverter and the output is the change in power angle and capacitor voltage of each inverter ( $\Delta\delta_i$  and  $\Delta v_{Ti}$ ). The corresponding relation is given as:

$$\begin{aligned} \Delta\omega_i &= -m_p * (\Delta P_{\text{funi}}) = -m_p * \left\{ \frac{\omega_c}{s + \omega_c} * (\Delta P_{\text{cali}}) \right\} \\ \Delta\delta_i &= \int \omega_i dt \\ \Delta v_{Ti} &= -n_q * (\Delta Q_{\text{funi}}) = -n_q * \left\{ \frac{\omega_c}{s + \omega_c} * (\Delta Q_{\text{cali}}) \right\} \end{aligned} \quad (32)$$

where

$$\Delta P_{\text{cali}} = \frac{1}{1 + s\tau} * \Delta P_{\text{insi}} \quad (33)$$

The instantaneous power ( $\Delta P_{\text{insi}}$ ) given above is the sum of initial power (discussed in step 1) and the dynamic power flow (calculation of which will be shown in further steps). Initially, when the dynamic power flow is zero, the instantaneous power becomes same as the initialised power.

**Table 4** Initial sharing of load powers

Load connected at bus	Inverter number	Expression for initial power	Numerical value
1 ( $P_{\text{Load}1}$ )	1	$P_{L1}^1 = P_{\text{Load}1} \times \text{mag}\left(\frac{Z_{\text{eq}1}}{Z_1 + Z_{\text{eq}1}}\right)$	$P_{L1}^1 = P_{\text{Load}1} \times 0.729$
1 ( $P_{\text{Load}1}$ )	2	$P_{L2}^1 = P_{\text{Load}1} \times \text{mag}\left(\frac{\frac{Z_1}{Z_1 + Z_{\text{eq}1}} \times Z_{\text{eq}2}}{Z_2 + Z_{\text{eq}2}}\right)$	$P_{L2}^1 = P_{\text{Load}1} \times 0.233$
1 ( $P_{\text{Load}1}$ )	3	$P_{L3}^1 = P_{\text{Load}1} \times \text{mag}\left(\frac{\frac{Z_1}{Z_1 + Z_{\text{eq}1}} \times Z_2}{Z_2 + Z_{\text{eq}2}}\right)$	$P_{L3}^1 = P_{\text{Load}1} \times 0.033$
2 ( $P_{\text{Load}2}$ )	1	$P_{L1}^2 = P_{\text{Load}2} \times \text{mag}\left(\frac{Z_{\text{eq}4}}{Z_{\text{eq}3} + Z_{\text{eq}4}}\right)$	$P_{L1}^2 = P_{\text{Load}2} \times 0.233$
2 ( $P_{\text{Load}2}$ )	2	$P_{L2}^2 = P_{\text{Load}2} \times \text{mag}\left(\frac{\frac{Z_{\text{eq}3}}{Z_{\text{eq}3} + Z_{\text{eq}4}} \times Z_{\text{eq}2}}{Z_2 + Z_{\text{eq}2}}\right)$	$P_{L2}^2 = P_{\text{Load}2} \times 0.697$
2 ( $P_{\text{Load}2}$ )	3	$P_{L3}^2 = P_{\text{Load}2} \times \text{mag}\left(\frac{\frac{Z_{\text{eq}3}}{Z_{\text{eq}3} + Z_{\text{eq}4}} \times Z_2}{Z_2 + Z_{\text{eq}2}}\right)$	$P_{L3}^2 = P_{\text{Load}2} \times 0.1$
3 ( $P_{\text{Load}3}$ )	1	$P_{L1}^3 = P_{\text{Load}3} \times \text{mag}\left(\frac{\frac{Z_3}{Z_3 + Z_{\text{eq}5}} \times Z_2}{Z_2 + Z_{\text{eq}6}}\right)$	$P_{L1}^3 = P_{\text{Load}3} \times 0.033$
3 ( $P_{\text{Load}3}$ )	2	$P_{L2}^3 = P_{\text{Load}3} \times \text{mag}\left(\frac{\frac{Z_3}{Z_3 + Z_{\text{eq}5}} \times Z_{\text{eq}6}}{Z_2 + Z_{\text{eq}6}}\right)$	$P_{L2}^3 = P_{\text{Load}3} \times 0.1$
3 ( $P_{\text{Load}3}$ )	3	$P_{L3}^3 = P_{\text{Load}3} \times \text{mag}\left(\frac{Z_{\text{eq}5}}{Z_3 + Z_{\text{eq}5}}\right)$	$P_{L3}^3 = P_{\text{Load}3} \times 0.873$

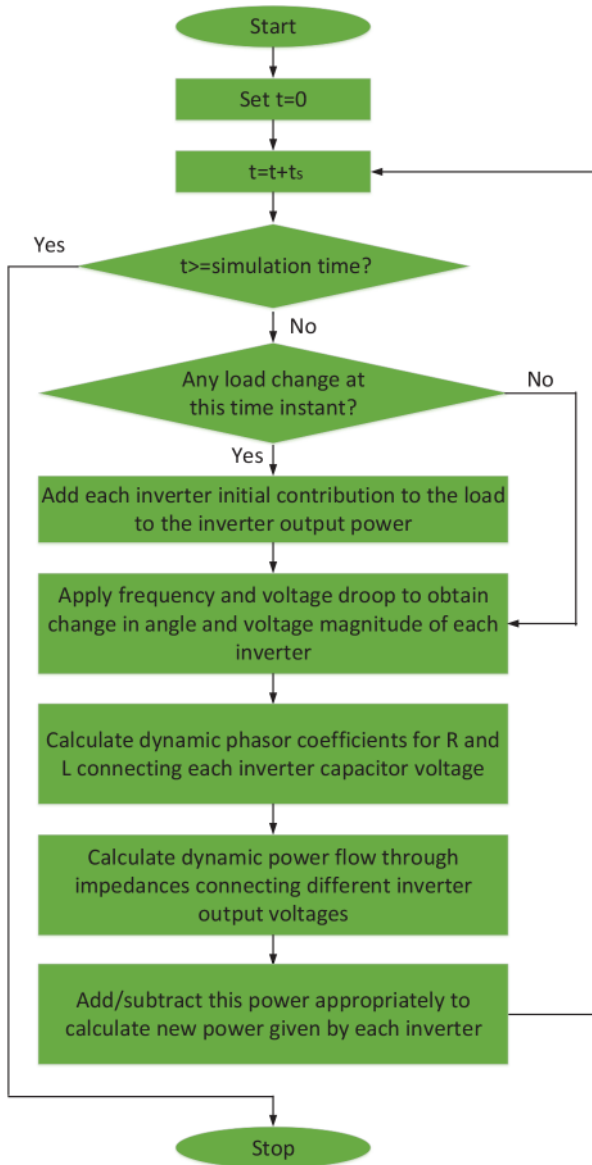


**Fig. 3** Flowchart representing step by step simulation procedure with the proposed method

A first-order transfer function, given in (33) is introduced in this path to account for the delay in the measurement of quantities and achieving the desired control. The time constant ( $\tau$ ) of this transfer function can be taken roughly close to half electrical cycles. For better accuracy this delay can be represented by  $e^{-s\tau}$  or its Padé approximation of appropriate order [27, 28].

(3) Third step is to find out the dynamic phasor coefficients using the inductance and resistance between the capacitor terminal voltage of inverters depending upon the initial operating voltages using the relation given in (27).

(4) Once the coefficients are known, the power flows between any set of inverters can be calculated using (7) as given in the following relations:

$$\begin{aligned} \Delta \tilde{p}_{n,n-1} &= f(\Delta v_{T_{n,n-1}}, \Delta \delta_{n,n-1}) \\ \Delta \tilde{p}_{n-1,n-2} &= f(\Delta v_{T_{n-1,n-2}}, \Delta \delta_{n-1,n-2}) \\ \Delta \tilde{p}_{n-2,n-3} &= f(\Delta v_{T_{n-2,n-3}}, \Delta \delta_{n-2,n-3}) \\ &\vdots \\ \Delta \tilde{p}_{2,1} &= f(\Delta v_{T_{2,1}}, \Delta \delta_{2,1}) \end{aligned} \quad (34)$$

where  $n$  = index of inverter. For example, for the system presented in this paper, there are three buses and two lines. So, the line flow equations are:

$$\begin{aligned} \Delta \tilde{p}_{3,2} &= f(\Delta v_{T_{3,2}}, \Delta \delta_{3,2}) \\ \Delta \tilde{p}_{2,1} &= f(\Delta v_{T_{2,1}}, \Delta \delta_{2,1}) \end{aligned} \quad (35)$$

In (34) and (35), the active power flow relations are given. Same process is to be followed for reactive power calculations as well. It is to be noted that in these equations it is assumed that power is flowing from higher numbered source to lower numbered source. If the power is actually flowing in the reverse direction, the dynamic power calculated above will appear negative.

Once the change in power flows are obtained, the change in power generated by each inverter can be calculated. If power is going out of the inverter bus, it signifies an increase in inverter power output while if power is coming into the inverter bus, it signifies a decrease in inverter output power. Thus, change in dynamic power generated by each inverter will be equal to the resultant change in power coming in or going out at the inverter bus. Mathematically, it can be presented as:

$$\Delta \tilde{P}_i = \sum \Delta \tilde{p}_{i,j} - \sum \Delta \tilde{p}_{k,i} \quad (36)$$

where  $\Delta \tilde{p}_{i,j}$  represents the dynamic power flowing out of the bus  $i$  and  $\Delta \tilde{p}_{k,i}$  represents the dynamic power flowing in to the bus  $i$ .

(5) The last step is to add the change in inverter power to the initial power to obtain the inverter instantaneous power (of each inverter) which is then given to the droop controller (step 2).

$$\Delta P_{\text{ins}i} = \Delta P_{\text{ini}i} + \Delta \tilde{P}_i \quad (37)$$

Thus, for the three inverter system considered in this work, the instantaneous power of each inverter can be written as follows:

$$\begin{aligned} \Delta P_{\text{ins}3} &= \Delta P_{\text{ini}3} + \Delta \tilde{P}_3 \\ \Delta P_{\text{ins}2} &= \Delta P_{\text{ini}2} + \Delta \tilde{P}_2 \\ \Delta P_{\text{ins}1} &= \Delta P_{\text{ini}1} + \Delta \tilde{P}_1 \end{aligned} \quad (38)$$

where

$$\begin{aligned} \Delta \tilde{P}_3 &= \Delta \tilde{p}_{3,2} \\ \Delta \tilde{P}_2 &= \Delta \tilde{p}_{2,1} - \Delta \tilde{p}_{3,2} \\ \Delta \tilde{P}_1 &= -\Delta \tilde{p}_{2,1} \end{aligned} \quad (39)$$

Reactive power generated by each inverter is calculated in the same way as the active power (discussed above) using the function  $g(\Delta v_{T_{i,j}}, \Delta \delta_{i,j})$ . The corresponding equations are similar to the active power equations and are not shown here to avoid redundancy. It is to be noted that line losses are neglected in this approach. The complete procedure for obtaining the time response from the simulation of the simplified small-signal model is also summarised in Fig. 3.

## 5 Results and discussions

To verify the procedure discussed above, detailed time-domain simulations and eigenvalue analysis for different test cases are presented and compared with the proposed model. The proposed model shows how power is shared equally at equal droop coefficients as well as it also able to find out the stability margin of the microgrid without detailed state-space modelling.

### 5.1 Time domain simulation

**5.1.1 When every bus is an inverter bus (three inverter system):** A simplified model for three inverter microgrid shown in Fig. 1a is developed and it is shown in Fig. 4. There are two loads connected at buses 1 and 3. Hence, the initial power of inverter 1, 2 and 3 is calculated as per their impedance ratio to the load as described in Section 4. The inverter 1 is taken as the reference inverter, therefore, the line flows from other inverters to the reference one are calculated as given in (39). The active power, inverter frequency, reactive power and  $d$ -axis inverter voltage of

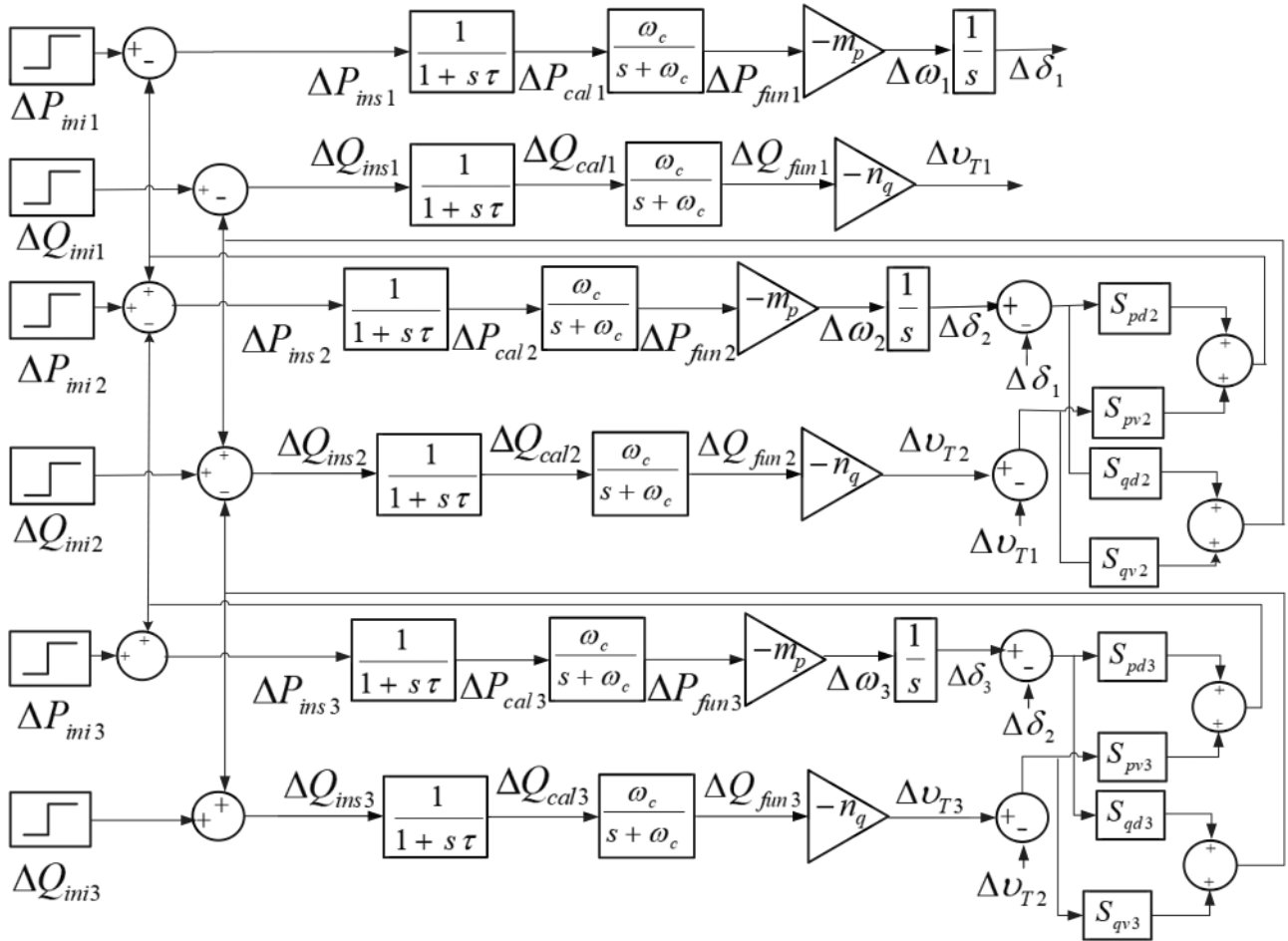


Fig. 4 Proposed simplified transfer function model

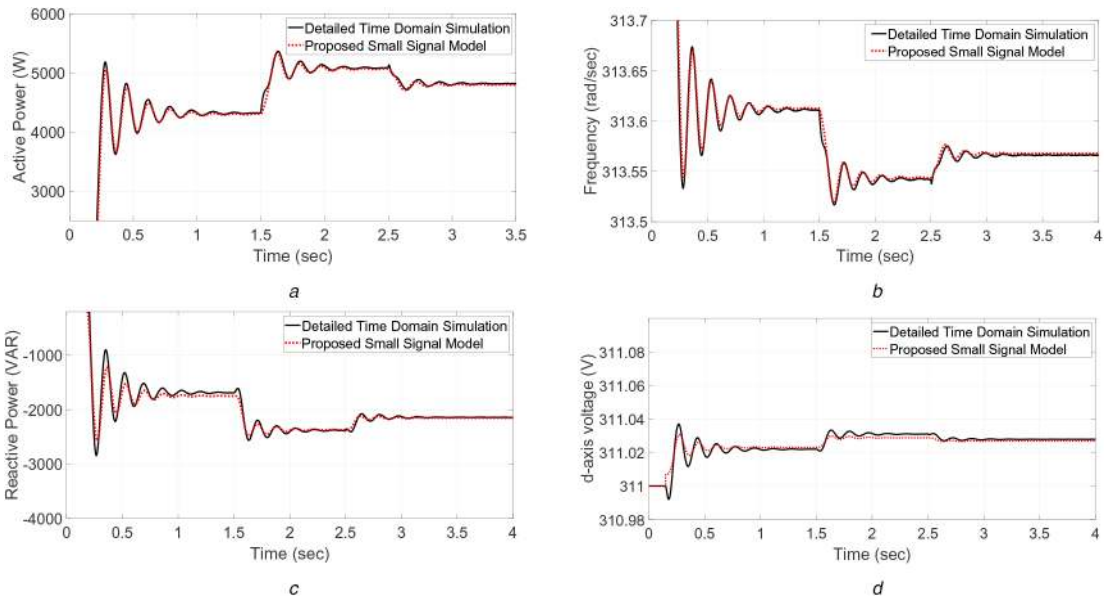


Fig. 5 Simulation results of detailed and proposed small signal model for three inverter microgrid

(a) Active power of inverter 2, (b) Frequency deviation of inverter 2, (c) Reactive power of inverter 2, (d) Voltage magnitude of inverter 2

inverter 2 obtained with detailed time-domain simulation using MATLAB/Simulink and with the proposed small-signal model are shown in Fig. 5. The results show that the proposed model is closely matching with the detailed time-domain simulation with different load perturbations at 1.5 and 2.5 sec. Results of other inverters are not shown to avoid redundancy.

The iterative loop shown in Fig. 3, gives the power of each inverter till the loop is running (up to simulation time). In each step, the power of the inverters are updated and this way the

proposed model also gives the result of power-sharing among the inverters which is normally obtained by simulation of the actual system which is complex and time consuming as the actual system is a non-linear one. As seen in Fig. 5, the simulation results obtained by the proposed method match satisfactorily with the actual simulation. Based on this, the power sharing and frequency deviation among all three inverters can be seen with the help of the proposed model as shown in Fig. 6. The proposed model accurately converges to a steady-state power-sharing between all three

inverters and hence, it can be used for power-sharing studies in place of detailed non-linear time-domain simulation.

The results shown in Fig. 5 are obtained by simulating the system for a duration of 4 s in MATLAB/Simulink at  $50 \mu\text{s}$  time step in a Windows 10 Computer with 2.60 GHz processors. The time taken to run the detailed simulation was 9 min and 4 s while the time taken to run the proposed small-signal model in the same computer was only 7 s. This shows the advantage of the proposed model in terms of computational efficiency.

**5.1.2 Effect of  $\tau$ :** It is shown in [27, 28] that time delay of the digital control must be taken into account when modelling the dynamics of the power control loop. This delay is actually represented by the transfer function  $e^{-sT}$  where  $T$  is the time period of the grid frequency. It is shown in [27, 28] that if  $e^{-sT}$  is replaced by the first-order Padé approximation, then the transfer function that relates the instantaneous power to the average power can be approximately given by  $(1)/(1 + (T/2)s)$ . Therefore, in this work, we have taken the time constant roughly close to the half-cycle time period. However, this might introduce some error and the time constant may need to be tuned to get more accurate results. Therefore, the time constant  $\tau$  may need to be computed analytically. The exact method to analytically compute this parameter will be taken as a future study by the authors.

In order to observe the effect of  $\tau$ , the droop coefficient,  $m_p$  is kept at the critical value obtained with  $\tau = 0.01$  (half of the

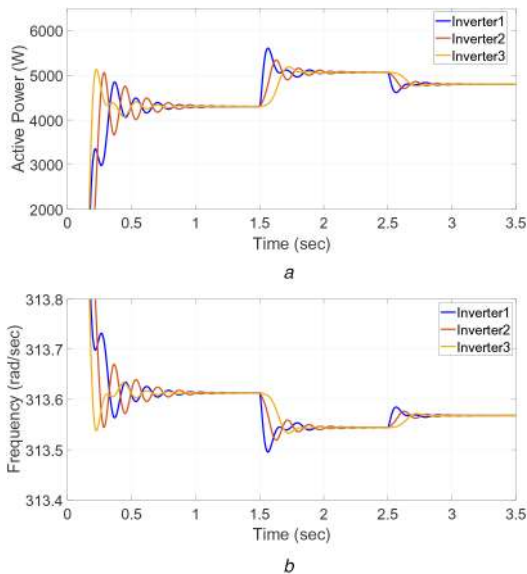


**Fig. 6** Simulation results for three inverter system with proposed model (a) Active power sharing of three inverters, (b) Frequency deviation of three inverters

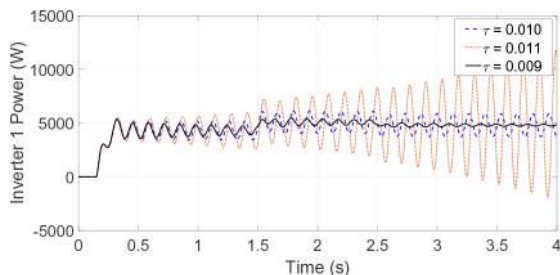


**Fig. 7** Effect of  $\tau$  on inverter 1 power

**Table 5** Effect of  $\tau$  on critical droop

$\tau$	Critical $m_p$
0.011	$1.4 \times 10^{-4}$
0.010	$1.48 \times 10^{-4}$
0.009	$1.61 \times 10^{-4}$

electrical time period) while the parameter  $\tau$  is changed. Results are compared at three different values of  $\tau$ . It is observed that more stable response is observed for lower values of  $\tau$  as shown in Fig. 7.

As more stable results are seen at lower  $\tau$  values, the critical droop values obtained are also different for different  $\tau$  values as shown in Table 5. Although the variation of critical droop is in a range close to the actual critical droop, however, these results show that the accuracy of the model may depend on the selection of  $\tau$ . As discussed earlier, in this work  $\tau$  is taken close to half-cycle time period but the exact method of calculating this parameter needs further investigation and it will be taken by authors in their future research.

**5.1.3 When one bus is not an inverter bus (two inverter system):**

The proposed model is also tested for a case when a non-inverter bus is present in a system. For this, inverter 2 of Fig. 1a is removed resulting in a two inverter system with three buses. Now the bus number 2 becomes a non-inverter bus. The proposed small-signal model of such a system can be easily obtained using the procedure given in Section 4. The only difference is that, now the two lines indicated by  $Z_{Line12}$  and  $Z_{Line23}$  in Fig. 1a are now added to make a single line which is used to calculate the dynamic power flows. Fig. 8 shows the comparison results for this system with detailed simulation and with proposed simulation. In this case, also, results are only shown for one inverter to avoid redundancy. The results clearly show a good match with the detailed simulation.

**5.1.4 Comparison with existing model:**

To show the comparison with existing methods, the proposed model is compared with the model presented in [23]. This is because both the models (the proposed model and the method presented in [23]) are based on dynamic phasor approach and both models provide a simple yet accurate model of the microgrid without involving complex mathematical tools. Rather [23] forms the basis of the proposed model and the improvements observed in the result as compared to [23] will help readers understand the significance of the proposed work.

Further, to make the comparison with [23], the 2 inverter system in Section 5.1.3 is considered with a load at the bus where the two lines meet. This is done to make the system similar to the one presented in [23] where both the sources are connected to a common bus through lines and load is connected to the same bus.

**Effect of dynamics of sources against each other:** The key difference in the model presented in [23] is that for each source its own voltage angle and magnitude are used to calculate active and reactive power by assuming the bus voltage magnitude and angle to be constant. On the contrary, the proposed model studies the oscillations among the various sources by using the difference of voltage magnitude and angle of the sources. This is a major improvement that the proposed model presents in comparison to the existing works. This comparison is shown in Fig. 9. It can be seen in the results that the proposed model accurately tracks the exact simulation results while there are significant oscillations if the system is modelled as per [23].

**Effect of exclusion of transfer function:** To show this comparison, the transfer function  $((1)/(1 + s\tau))$  is removed from the proposed model (similar to [23]) while other aspects of the model are kept constant. The response of the system with the proposed model and the proposed model without the transfer function (similar to [23]) are compared with the detailed time-domain simulation of the actual system at a random droop coefficient and the results are presented in the Fig. 10. It can be seen from the results that if the transfer function is not considered,

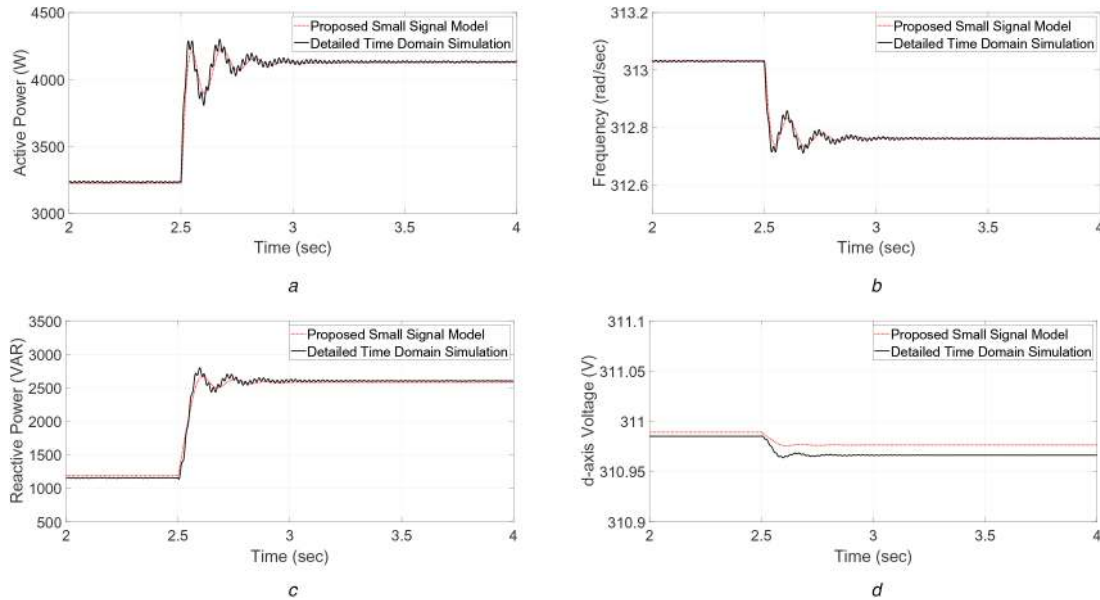


**Fig. 8** Simulation results of detailed and proposed small signal model as per system in Section 5.1.3  
 (a) Active power of inverter 1, (b) Frequency deviation of inverter 1, (c) Reactive power of inverter 1, (d) Voltage magnitude of inverter 1

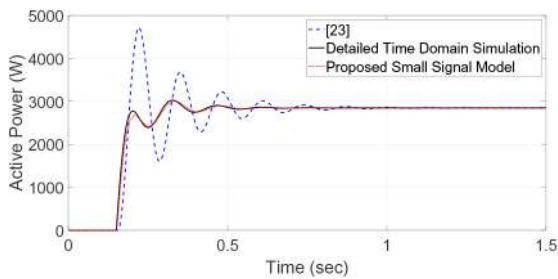


**Fig. 9** Effect of modelling process on inverter 1 power

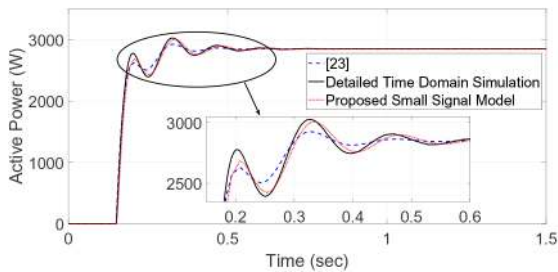


**Fig. 10** Effect of exclusion of  $\tau$  on inverter 1 power

**Table 6** Effect of considering delay transfer function on critical droop

Model	Critical $m_p$
detailed time domain simulation	$6.3 \times 10^{-4}$
proposed	$7.1 \times 10^{-4}$
without $\tau$	$14.9 \times 10^{-4}$

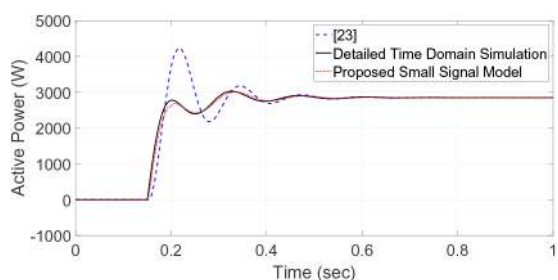


**Fig. 11** Comparison of inverter 1 power with different methods

more stable results are seen. This is in line with the above results that reduction of  $\tau$  results in a more stable response. This leads to significant error in the critical droop value as compared to the proposed model as shown in Table 6.

**Combined effect:** It is seen from the above results that the method presented in [23] gives two drawbacks. First, more oscillations are seen if the modelling used in [23] is used. On the contrary, in the second case, due to exclusion of the delayed transfer function more stable results are seen. The two effects are opposite to each other and the combined effect of the two is also compared with the proposed model by using both the two together, i.e. considering exclusion of the delay transfer function and considering the dynamics of the sources against a fixed bus together to make the model resemble the model proposed in [23]. The results are shown in Fig. 11. The results clearly show that the stabilising effect of exclusion of delay transfer function helps in reducing the oscillations in the system but the overall response still shows larger oscillations in comparison to the actual response while the proposed model gives more or less accurate results.

## 5.2 Eigen value analysis of proposed model

Eigenvalue analysis for the two cases described in the previous section is carried out using linear analysis toolbox of MATLAB to compare the stability limits and frequency modes of detailed small signal model and proposed small signal model.

**5.2.1 When every bus is an inverter bus:** For the three inverter microgrid system of Fig. 1a, eigenvalues are calculated. It is shown that there are two critical low-frequency modes in the system as tabulated in Table 2 as per the detailed small signal modelling. The eigenvalues obtained from the proposed model also show the critical low-frequency modes. Fig. 12 shows the trace of both modes on varying  $m_p$  and  $n_q$ . When  $m_p$  is increased up to a certain value at fixed  $n_q$ , the system becomes unstable due to the shifting of the mode-1 from left half to the right half of the s-plane as shown in Fig. 12a. Mode-2 also shifts towards the right (Fig. 12a), but due to the higher damping than mode-1, its movement is slower. Similarly, shifting of both the modes with varying  $n_q$  is also shown in Fig. 12b. Based on these traces, it can be concluded that there exists a critical droop value ( $m_p$ ) for which the system is marginally stable. The comparison of the critical droop and the corresponding eigenvalue using both the model of Sections 3 and 4 are tabulated in Table 7. From the results shown in Table 7, it is found that the proposed model identifies the two critical modes as well as the system stability limit with acceptable accuracy. Hence, the proposed model is also able to predict the low-frequency modes

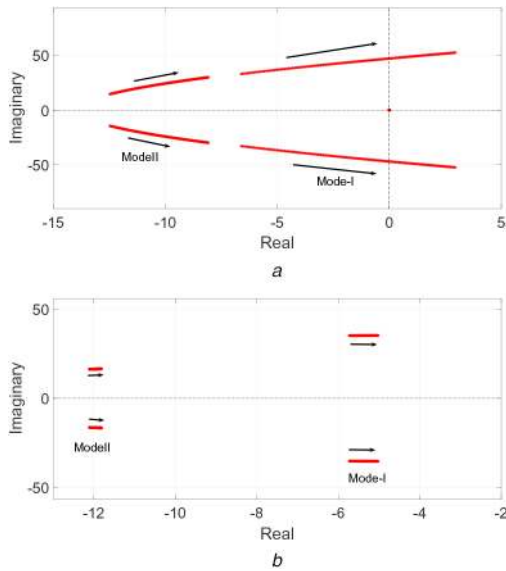


**Fig. 12** Eigen value trace of dominant low-frequency modes for three inverter system

(a) Trace of mode I and mode II  $m_p$  is increased at  $n_q = 1.3 \times 10^{-5}$ , (b) Trace of mode I and mode II system  $n_q$  is increased at  $m_p = 9 \times 10^{-5}$

and their sensitivity to droop parameters accurately for stability analysis. Without going into detailed computational modelling, the proposed model effectively calculates the results with very less computation.

**5.2.2 When one bus is not an inverter bus:** Eigenvalue analysis is also carried out for two inverter system using the detailed and proposed small-signal method. The trace of critical low-frequency mode for this system is shown in Fig. 13 and the comparison of critical droop value is also shown in Table 8. It is found that the proposed model also works well in identifying stability limit and frequency modes for this system making the proposed model more generic and simple for different configuration of microgrids.

From the simulation and eigen-value results, it is concluded that the proposed model not only predicts the system stability but also gives acceptable transient response in the time domain. Therefore, the proposed model can be used to simulate larger radial microgrids with passive loads by using linear transfer functions only.

### 5.3 Discussion

The approach presented in this paper has been implemented for two configurations of the microgrid. However, the method can be easily applied in any other configuration of droop controlled inverter-based microgrid using the three simple steps:

- Initialise the powers
- Calculate the dynamic power coefficients
- Appropriately add/subtract the power flowing from one source to the another. For a new source, it will only affect its neighbouring source while the rest will not change. Hence, the approach is easily scalable.

## 6 Conclusion

This paper presents a simplified small signal stability analysis approach based on dynamic power flow for inverter-based isolated microgrids. Conventionally small-signal state space analysis is used to calculate the low-frequency modes of the system. However, the process is very complex and involves large computations for larger systems. Therefore, for stability studies, this work proposes a step by step procedure for developing an AGC-based simplified model to calculate the stability margin and the various low-frequency modes present in isolated microgrids. Dynamic phasor based representation of the network is used to calculate the line

**Table 7** Stability limit and frequency modes for three inverter system

Type of model	Critical stability limit ( $m_p$ )	Critical low-frequency modes
detailed small signal [4]	$1.15 \times 10^{-4}$	mode I = $-0.02 \pm 49.27j$ ; mode II = $-12.91 \pm 29.18j$
proposed small signal	$1.48 \times 10^{-4}$	mode I = $-0.29 \pm 46.52j$ ; mode II = $-10.31 \pm 26.43j$

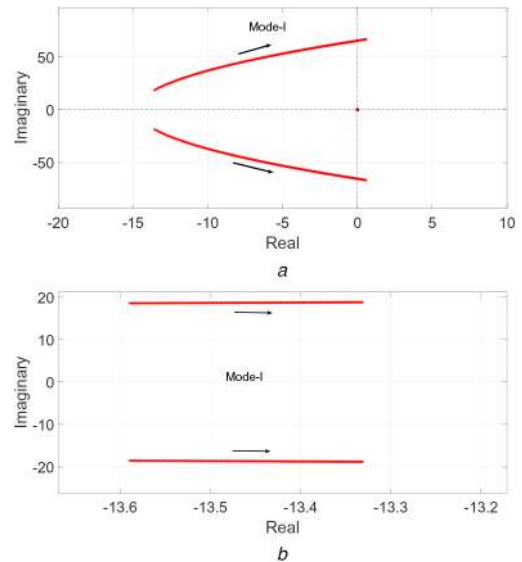


**Fig. 13** Eigen value trace of dominant low-frequency modes for two inverter system

(a) Trace of mode I when  $m_p$  is increased at  $n_q = 1.3 \times 10^{-5}$ , (b) Trace of mode I when  $n_q$  is increased at  $m_p = 9 \times 10^{-5}$

**Table 8** Stability limit and frequency modes for two inverter system

Type of model	Critical stability limit ( $m_p$ )	Critical low-frequency modes
detailed small signal [4]	$6.3 \times 10^{-4}$	mode I = $-0.06 \pm 68.98j$
proposed small signal	$7.1 \times 10^{-4}$	mode I = $-0.15 \pm 65.2j$

power flows which follow network dynamics. Other than the network, dynamics of droop controller of the inverter is considered for analysis. The process is much easier as compared to the conventional modelling and it can work effectively as verified by the time domain simulation results as well as by eigenvalue analysis. The added advantage obtained with this model is that it not only provides a simplified system for study but is also provides the flexibility of doing time-domain simulations as well as  $s$ -domain analysis with the same system as it is a linear transfer function-based model. Therefore, the proposed modelling algorithm can be used for easier stability analysis of the larger systems having a large number of inverters with distributed passive loads. The accuracy of the model depends on the selection of the time constant  $\tau$ . Although the value close to half electrical cycle is sufficiently accurate for inverter-based systems, the exact method of selection of the time constant will be taken by the authors as a future work.

## 7 Acknowledgments

This work was supported in part by the Science & Energy Research Board (SERB), Department of Science & Technology (DST), Govt. of India through the Distinguished Investigator Award (DIA) scheme (File number - DIA/2018/000032).

## 8 References

- [1] Majumder, R.: 'Some aspects of stability in microgrids', *IEEE Trans. Power Syst.*, 2013, **28**, (3), pp. 3243–3252
- [2] Chandorkar, M.C., Divan, D.M., Adapa, R.: 'Control of parallel connected inverters in standalone ac supply systems', *IEEE Trans. Ind. Appl.*, 1993, **29**, (1), pp. 136–143
- [3] Coelho, E.A.A., Cortizo, P.C., Garcia, P.F.D.: 'Small-signal stability for parallel-connected inverters in stand-alone ac supply systems', *IEEE Trans. Ind. Appl.*, 2002, **38**, (2), pp. 533–542
- [4] Pogaku, N., Prodanovic, M., Green, T.C.: 'Modeling, analysis and testing of autonomous operation of an inverter-based microgrid', *IEEE Trans. Power Electron.*, 2007, **22**, (2), pp. 613–625
- [5] Barklund, E., Pogaku, N., Prodanovic, M., *et al.*: 'Energy management in autonomous microgrid using stability-constrained droop control of inverters', *IEEE Trans. Power Electron.*, 2008, **23**, (5), pp. 2346–2352
- [6] Kahrobaei, A., Mohamed, Y.A.R.I.: 'Analysis and mitigation of low-frequency instabilities in autonomous medium-voltage converter-based microgrids with dynamic loads', *IEEE Trans. Ind. Electron.*, 2014, **61**, (4), pp. 1643–1658
- [7] Bottrell, N., Prodanovic, M., Green, T.C.: 'Dynamic stability of a microgrid with an active load', *IEEE Trans. Power Electron.*, 2013, **28**, (11), pp. 5107–5119
- [8] Vijay, A.S., Dheer, D.K., Tiwari, A., *et al.*: 'Performance evaluation of homogeneous and heterogeneous droop-based systems in microgrid—stability and transient response perspective', *IEEE Trans. Energy Convers.*, 2019, **34**, (1), pp. 36–46
- [9] Raman, G.P., Peng, J.C.: 'Mitigating stability issues due to line dynamics in droop-controlled multi-inverter systems', *IEEE Trans. Power Syst.*, 2020, **35**, (3), pp. 2082–2092
- [10] Firdaus, A., Mishra, S.: 'Mitigation of power and frequency instability to improve load sharing among distributed inverters in microgrid systems', *IEEE Systems Journal*, 2020, **14**, (1), pp. 1024–1033
- [11] Mohamed, Y.A.R.I., El-Saadany, E.F.: 'Adaptive decentralized droop controller to preserve power sharing stability of paralleled inverters in distributed generation microgrids', *IEEE Trans. Power Electron.*, 2008, **23**, (6), pp. 2806–2816
- [12] Majumder, R., Chaudhuri, B., Ghosh, A., *et al.*: 'Improvement of stability and load sharing in an autonomous microgrid using supplementary droop control loop', *IEEE Trans. Power Syst.*, 2010, **25**, (2), pp. 796–808
- [13] Aderibole, A., Zeineldin, H.H., Hosani, M.A.: 'A critical assessment of oscillatory modes in multi-microgrids comprising of synchronous and inverter based distributed generation', *IEEE Trans. Smart Grid*, 2019, **10**, (3), pp. 3320–3330
- [14] Dheer, D.K., Vijay, A.S., Kulkarni, O.V., *et al.*: 'Improvement of stability margin of droop-based islanded microgrids by cascading of lead compensators', *IEEE Trans. Ind. Appl.*, 2019, **55**, (3), pp. 3241–3251
- [15] Hassan, M.A., Abido, M.A.: 'Optimal design of microgrids in autonomous and grid-connected modes using particle swarm optimization', *IEEE Trans. Power Electron.*, 2011, **26**, (3), pp. 755–769
- [16] Yu, K., Ai, Q., Wang, S., *et al.*: 'Analysis and optimization of droop controller for microgrid system based on small-signal dynamic model', *IEEE Trans. Smart Grid*, 2016, **7**, (2), pp. 695–705
- [17] Hassan, M.A.: 'Dynamic stability of an autonomous microgrid considering active load impact with a new dedicated synchronization scheme', *IEEE Trans. Power Syst.*, 2018, **33**, (5), pp. 4994–5005
- [18] Luo, L., Dhople, S.V.: 'Spatiotemporal model reduction of inverter-based islanded microgrids', *IEEE Trans. Energy Convers.*, 2014, **29**, (4), pp. 823–832
- [19] Mariani, V., Vasca, F., Vásquez, J.C., *et al.*: 'Model order reductions for stability analysis of islanded microgrids with droop control', *IEEE Trans. Ind. Electron.*, 2015, **62**, (7), pp. 4344–4354
- [20] Rasheduzzaman, M., Mueller, J.A., Kimball, J.W.: 'Reduced-order small-signal model of microgrid systems', *IEEE Trans. Sustain. Energy*, 2015, **6**, (4), pp. 1292–1305
- [21] Nikolakakos, I.P., Zeineldin, H.H., Moursi, M.S.E., *et al.*: 'Reduced-order model for inter-inverter oscillations in islanded droop-controlled microgrids', *IEEE Transactions on Smart Grid*, 2018, **9**, (5), pp. 4953–4963
- [22] Nikolakakos, I.P., Zeineldin, H.H., El-Moursi, M.S., *et al.*: 'Stability evaluation of interconnected multi-inverter microgrids through critical clusters', *IEEE Trans. Power Syst.*, 2016, **31**, (4), pp. 3060–3072
- [23] Guo, X., Lu, Z., Wang, B., *et al.*: 'Dynamic phasors-based modeling and stability analysis of droop-controlled inverters for microgrid applications', *IEEE Transactions on Smart Grid*, 2014, **5**, (6), pp. 2980–2987
- [24] Kundur, P., Balu, N.J., Lauby, M.G.: '*Power system stability and control*' (McGraw-hill, New York, 1994)
- [25] Elgerd, O.I.: '*Electric energy systems theory: an introduction*' (Tata McGrawHill, New Delhi, India, 1982)
- [26] Maksimovic, D., Stankovic, A.M., Thottuvelil, V.J., *et al.*: 'Modeling and simulation of power electronic converters', *Proc. IEEE*, 2001, **89**, (6), pp. 898–912
- [27] Vasquez, J.C., Guerrero, J.M., Luna, A., *et al.*: 'Adaptive droop control applied to voltage-source inverters operating in grid-connected and islanded modes', *IEEE Trans. Ind. Electron.*, 2009, **56**, (10), pp. 4088–4096
- [28] Wang, R., Sun, Q., Zhang, P., *et al.*: 'Reduced-order transfer function model of the droop-controlled inverter via jordan continued-fraction expansion', *IEEE Trans. Energy Convers.*, 2020, **35**, (3), pp. 1585–1595